Creasing to Cratering Instability in Polymers under Ultrahigh Electric Fields

Qiming Wang, Lin Zhang, and Xuanhe Zhao*

Soft Active Materials Laboratory, Department of Mechanical Engineering and Materials Science, Duke University, Durham, North Carolina 27708, USA

(Received 22 November 2010; published 14 March 2011)

We report a new type of instability in a substrate-bonded elastic polymer subject to an ultrahigh electric field. Once the electric field reaches a critical value, the initially flat surface of the polymer locally folds against itself to form a pattern of creases. As the electric field further rises, the creases increase in size and decrease in density, and strikingly evolve into craters in the polymer. The critical field for the electrocreasing instability scales with the square root of the polymer's modulus. Linear stability analysis overestimates the critical field for the electrocreasing instability. A theoretical model has been developed to predict the critical field by comparing the potential energies in the creased and flat states. The theoretical prediction matches consistently with the experimental results.

DOI: 10.1103/PhysRevLett.106.118301 PACS numbers: 82.35.Lr, 61.41.+e, 77.84.Jd

Introduction.—Formation of instability structures in polymers under electric fields is of great interest to various scientific and technological applications including insulating cables [1], organic capacitors [2], polymer actuators [3,4] and energy harvesters [5], and functional surfaces and patterns [6–8]. Previous studies on electric-field-induced instabilities in polymers mostly involve applying an electric field through an air gap to one or multiple layers of polymers bonded on a rigid substrate [6–10]. The permeability difference between air and polymers drives the instability process, competing with surface tension and/or elasticity of the polymers [11]. As a result, patterns of pillars and strips usually forms on the polymer surface [6–10]. For an elastic polymer, the critical field for the instability scales with the square root of the polymer's modulus [11]. The electrical breakdown of the air gap, however, limits the maximum applied field to the order of 10^6 V/m.

What happens when an electric field is applied, without the air gap, directly to a layer of a polymer bonded on a substrate [12]? The answer to this question will greatly extend the basic understanding of voltage-induced instabilities in polymers. The issue is also of fundamental importance in studying failures of polymers under voltages [1,13]. In this Letter, we present a combined experimental and theoretical study of a new type of instability in a substrate-bonded elastic polymer directly under an ultrahigh electric field up to 10^8 V/m. We show that the polymer film can evolve into a pattern of creases and/or craters, which are in distinct contrast to the previous observations [6–10].

Materials and methods.—The experimental setup for studying the new instability is shown in Fig. 1. A rigid polymer, Kapton, (DuPont, USA) with Young's modulus of 2.5 GPa and thickness of 125 μm was bonded on a metal substrate with conductive epoxy (SPI, USA). A polydimethyl siloxane (PDMS) based elastomer, Sylgard 184 (Dow Corning, USA) was spin coated on the Kapton film and cross-linked at 65 °C for 12 h. The cross-linker percentage in the elastomer was varied from 2% to 5% to give a shear modulus ranging from 6.7 to 155 kPa [Fig s1(a) [14]]. PDMS films of thickness from 40 to 212 μm were obtained by varying the spin coating speed from 3000 to 500 rpm [Fig s1(b) [14]]. The PDMS film was immersed in a transparent conductive solution (20 wt % NaCl solution) to observe the film deformation from a microscope (Nikon, Japan) above the solution. The conductive solution also acted as a conformal electrode that maintains contact with the PDMS film during its deformation. A high voltage supply (Matsusada, Japan) with controllable ramping rate was used to apply a voltage between the metal substrate and the conductive solution. The deformation of the Kapton film under applied voltages is negligible in comparison to PDMS' deformation, because the modulus of Kapton is over 3 orders of magnitude higher than those of PDMS films. Instead, the Kapton acts as a buffer substrate that prevents the electric field in the deformed PDMS film to become excessively high. Excessively high fields cause the electrical breakdown of the polymer film before instability patterns can be observed [13,15].

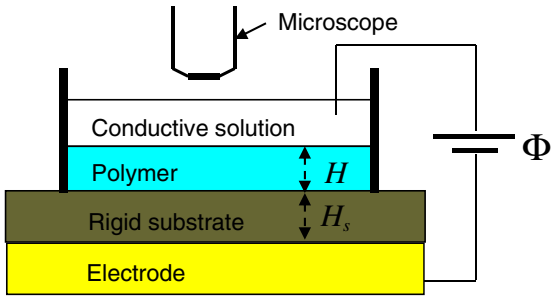

FIG. 1 (color online). The experimental setup for observing the electrocreasing to cratering instability.

Results.—Figure 2 illustrates the evolution of instability structures in a PDMS film subject to a ramping voltage with a rate of 10 V/s. See also video s1 of the supplemental material [14]. The surface of the PDMS film initially maintains a flat and smooth state without appreciable deformation [Fig. 2(a)]. When the voltage reaches a critical value, some regions of the PDMS surface suddenly fold upon themselves to form a pattern of creases as shown in Figs. 2(b) and 2(h). As the voltage increases, the pattern of creases coarsens by increasing their sizes (i.e., length and width) and decreasing their densities (i.e., number of creases per area) as shown on Fig. 2(c). As the voltage further rises, the center regions of some creases strikingly open, and a pattern of coexistent creases and craters form in the PDMS film [Fig. 2(d)]. The thickness of the film within the crater is less than the surrounding regions as illustrated in Fig. 2(i). All creases eventually deform into craters with further increase of the voltage [Fig. 2(e)]. The diameters of the craters increase, as the applied voltage further rises [Fig. 2(f)]. The PDMS film may also be fractured at the craters due to large deformation.

We first qualitatively explain the instability process by discussing its driving force. Creasing instability has been widely observed on surfaces of soft materials under compression. Examples include bending an elastomer bar [16–18], compressing a polymer foam [19], rising a bread dough in a bowl [20], and swelling a polymer gel bonded on a rigid substrate [21–23]. The creasing instability involves local folds of the surfaces without fracturing the materials [16–23]. For the first time, we show that the creasing to cratering instability occurs in a substrate-bonded polymer under an electric field. The driving force for the instability process is the electric-field-induced stress in the film. Given the dielectric behavior of PDMS is liquidlike, unaffected by deformation, the electric-field-induced stress can be expressed as [24]

$$\sigma_{ij}^{E} = \varepsilon E_i E_j - \tfrac{1}{2}\varepsilon E_k E_k \delta_{ij}, \tag{1}$$

where ε is the permittivity of PDMS, and $\mathbf{E}$ the electric field in the film. The electric field induces a tensile stress along the field, and a biaxial compressive stress normal to the field. As shown on Fig. 2(g), when the PDMS film is in a flat state, the applied electric field is normal to the film with a magnitude

$$E = \frac{\Phi}{H + H_s \varepsilon/\varepsilon_s}, \tag{2}$$

where Φ is the applied voltage, ε_s is the permittivity of Kapton, and H and H_s are the thicknesses of the PDMS film and Kapton substrate, respectively.

The electric field induces a biaxial compressive stress parallel to the film, as indicated on Fig. 2(g). When the compressive stress in the PDMS film reaches a critical value, creases develop on the surface of the film. The compressive stress increases with the applied electric field, and drives the coarsening of the creases. Similar phenomena of crease coarsening have been observed in gels bonded on rigid substrates, due to the increase of in-plane compressive stresses as the gels swell [21,22]. In the current experiment, the folded surfaces of creases in the PDMS film also act as electrodes lying vertically in the film [Fig. 2(h)]. Since the electric field is normal to the electrodes, the field induces a tensile stress perpendicular to the crease surfaces as illustrated in Fig. 2(h). The electrical tensile stress competes with the mechanical compressive stress, tending to pull the folded surface open. When the applied electric field is high enough, the creases deform into craters [Fig. 2(i)]. The diameters of the craters increase, as the electrical tensile stress further rises.

Scaling analysis.—We now analyze the instability through scaling. Let us consider the scales of various types of energies in a creased region as shown in Fig. 2(h). The electrostatic energy per unit thickness of the region around a crease is $\sim\varepsilon E^2 L^2$, where L is the depth of the crease. The elastic and surface energies per unit thickness of the crease region are $\sim\mu L^2$ and $\sim\gamma L$ respectively, where μ is the shear modulus of the PDMS film and γ the surface tension of PDMS in water. The decrease of the electrostatic energy drives the instability process, competing with the increase of the elastic and surface energies. If the elastic energy dominates over the surface energy, balancing the elastic and electrostatic energies gives the critical electric field

$$E_c \sim \sqrt{\mu/\varepsilon}. \tag{3}$$

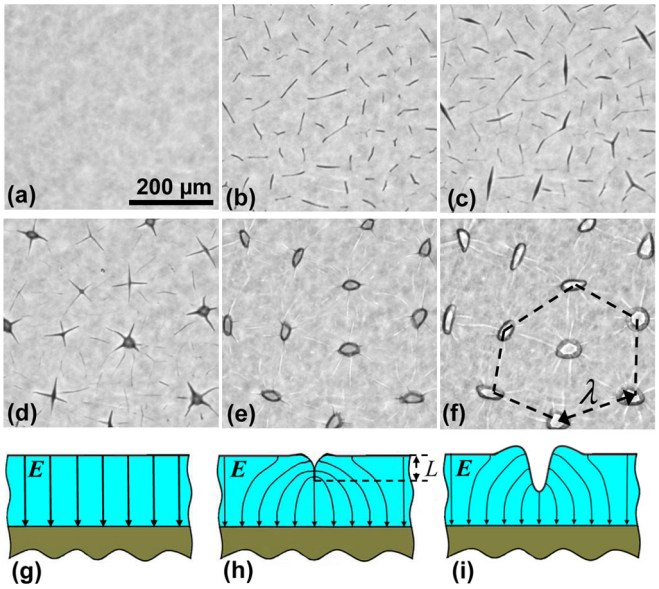

FIG. 2 (color online). Instability evolution in a substrate-boned PDMS film under a ramping voltage: flat state at 7 kV (a), creased state at 8.8 kV (b), crease coarsening at 9.7 kV (c), coexistent states of creases and craters at 10.5 kV (d), crater state at 13.3 kV (e), and craters with larger diameters at 15.6 kV (f). Schematic illustrations of the electric fields in a region at flat (g), creased (h), and crater (i) states.

On the other hand, if the surface energy dominates over the elastic energy, balancing the surface and electrostatic energies gives

$$E_c \sim \sqrt{\gamma/(\varepsilon L)}. \quad (4)$$

The PDMS films have $\gamma \approx 4 \times 10^{-2}$ Nm^{-1} [25], $\mu \approx$ 10–200 kPa, and $H \approx$ 40–200 μm. Assuming L to be 10 μm, a small fraction of H, it can be seen that the elastic energy is dominant over the surface energy. Therefore, the critical field for the electrocreasing instability should scale as Eq. (3). The critical voltages Φ_c for the electrocreasing instability experimentally measured in films with various thicknesses and moduli are given in Fig. 3(a). For films with the same modulus, the critical voltage scales linearly with the film thickness. The critical electric fields E_c are calculated using Eq. (2) with $H_s = 125$ μm, $\varepsilon_s = 3.5\varepsilon_0$, and $\varepsilon = 2.65\varepsilon_0$ [26], where the permittivity of vacuum $\varepsilon_0 = 8.85 \times 10^{-12}$ Fm^{-1}. From Fig. 3(b), it is evident that E_c is linear with $\sqrt{\mu/\varepsilon}$. The experimental results prove that the critical field for the electrocreasing instability is scaled as Eq. (3).

When the electric field reaches certain value higher than E_c, the crater has the same energy as the crease, and a pattern of coexistent creases and craters sets in [Fig. 2(d)]. As the electric field further rises, the craters become energetically favorable. The craters locally arrange into polygons, where the wavelengths λ of the craters are almost constant throughout the film as shown on Figs. 2(e) and 2(f). The decrease of the electrostatic energy tends to have a larger number of craters by reducing the wavelength. As the craters approach one another, the interaction of their strain fields increases the elastic energy, which prevents further reduction of the wavelength. The length scale for the interaction is the depth of the crater, which is roughly the film thickness. Thus the wavelength is scaled with the film thickness, i.e., $\lambda \sim H$. The experimental data in Fig. 3(c) give $\lambda \approx 1.5H$, independent of the moduli of the films.

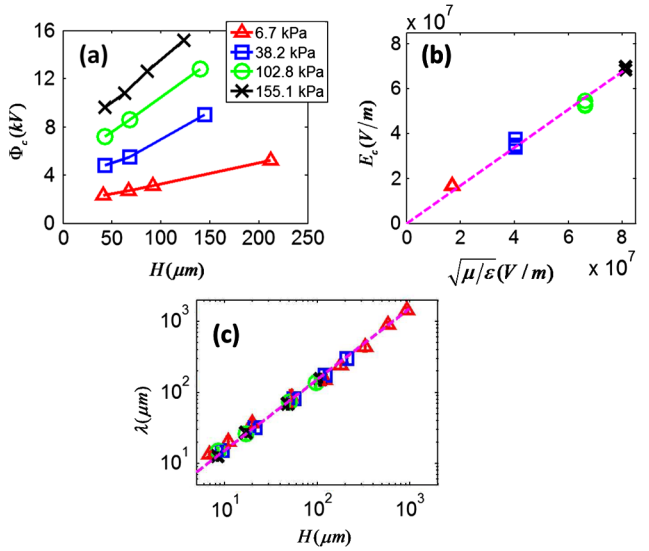

FIG. 3 (color online). The critical voltages (a) and electric fields (b) for the electrocreasing instability, and the wavelengths of the craters (c) in films with various thicknesses and moduli.

Theoretical calculation.—Now we calculate the critical field for the electrocreasing instability by comparing the potential energies in a region of the film in the flat and creased states [20,27]. Because the polymer substrate does not affect the critical field, we neglect the substrate in the calculation. The potential energy in a unit thickness of the region can be expressed as

$$\Pi = \int_A W(\mathbf{F}) dA + \int_A \frac{1}{2}\varepsilon|\mathbf{E}|^2 dA - \int_S \Phi\omega dS, \quad (5)$$

where $\mathbf{F}$ is the deformation gradient, $W(\mathbf{F})$ is the elastic energy density, ω is the surface charge density, and A and S are the area and contour of the region. The first term of Eq. (5) gives the elastic energy, and the second and third terms give the electrostatic potential energy of the region. Considering the *scaling analysis*, we neglect the surface energy of the film.

When the film is in a flat state, the elastic energy is zero and the electric field is uniform. The potential energy per unit thickness can be calculated as $\Pi_{\text{flat}} = -A\varepsilon E^2/2$, where E is given by Eq. (2). Next, we prescribe a downward displacement L to a line on the top surface of the region to form a crease as demonstrated in Fig. 4(a) [28]. At the creased state, the deformation and electric field are nonuniform in the region. We analyze the coupled deformation and electric field using finite-element software, ABAQUS 6.10.1 with a user subroutine UMAT. The potential energy of the creased state Π_{crease} is then calculated using Eq. (5). The program code is validated by a benchmark calculation shown in Fig s2 of the supplemental material [14], and the mesh accuracy is ascertained through a mesh refinement study. The region is taken to deform under plain-strain conditions, and obey the neo-Hookean model with the elastic energy density $W = \mu(F_{iK}F_{iK} - 3)/2$. Because of symmetry, only the right half of the region is calculated. The size of the calculation region is taken to be much larger (100 times) than the size of the crease, so that L is the only length scale relevant in comparing the potential energies in the flat and creased states [27]. [It should be noted that Fig. 4(a) only demonstrates a

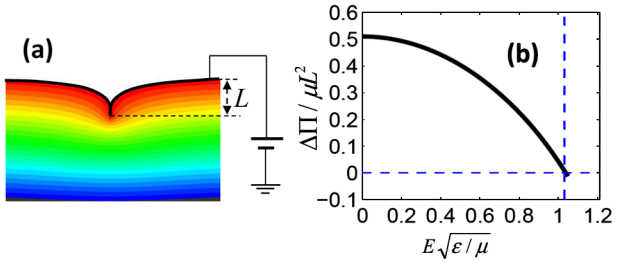

FIG. 4 (color online). The equipotential contours in a film at the creased state calculated from the finite-element model (a), and the potential energy difference between the creased and flat states as a function of the applied electric field (b).

small portion of the calculation domain.] The dimensional consideration determines that the potential energy difference has a form [27]

$$\Delta\Pi = \Pi_{\text{crease}} - \Pi_{\text{flat}} = \mu L^2 f(E\sqrt{\varepsilon/\mu}), \qquad (6)$$

where $f(E\sqrt{\varepsilon/\mu})$ is a dimensionless function of the applied electric field given by Eq. (2). The potential energy difference is plotted as a function of the applied electric field in Fig. 4(b). In absence of the applied field, the potential energy difference is positive, because $\Pi_{\text{flat}} = 0$ and the elastic energy of the crease gives a positive Π_{crease}. Thus the flat state is energetically preferable. As the applied electric field increases, the potential energy difference decreases, for the creased state has a lower electrostatic potential energy than the flat state. Once the electric field reaches a critical value E_c, the creased state has the same potential energy as the flat state (i.e., $\Delta\Pi = 0$) and the creasing instability sets in [17,20,27]. As shown in Fig. 4(b), the theoretical calculation gives $E_c \approx 1.03\sqrt{\mu/\varepsilon}$. From Fig. 3(b), the experimentally measured critical field for the electrocreasing instability is about $0.85\sqrt{\mu/\varepsilon}$. The theoretically predicted critical field is roughly consistent with the experimental data. The difference between the theoretical and experimental results may be due to the surface roughness of the PDMS films, and/or the deviation of the films' dielectric and elastic behaviors from the assumed ones.

Linear perturbation has been extensively used for analyzing instabilities in polymers under electric fields [11,24,29–31]. On the other hand, it has been shown that the creasing instability in a block of an elastomer under compression may not be analyzed with linear perturbation, since the strain around the crease tip is finite [17,20,27]. In Fig s3 of the supplemental material, we perform a linear perturbation analysis on a substrate-bonded elastic film under an electric field [30]. The critical field from the linear perturbation is $\sqrt{2\mu/\varepsilon}$, which overestimates the value calculated from the above analysis by 40%. This is consistent with previous reports that Biot's linear stability analysis overestimates the critical strain for the creasing instability in a block of an elastomer under compression [17,20,27,32].

Conclusion.—We report the voltage-induced creasing to cratering instability in an elastic polymer film bonded on a rigid substrate. When the film is in a flat state, the electric field induces an in-plane biaxial compressive stress, which can cause the creasing instability. After a crease is formed, the electric field induces a tensile stress normal to the crease surfaces, tending to pull the creases open into craters. We predict the critical electric field for the electrocreasing instability by comparing the potential energies in the creased and flat states. The theoretical prediction matches consistently with the experimental results. It is the first time that the electrocreasing to cratering instability has been observed and analyzed. Understanding this new instability is potentially useful in designing better insulating cables, organic capacitors, polymer actuators and energy harvesters, and functional surfaces and patterns.

We acknowledge the startup funds from the Pratt School of Engineering at Duke University. Q. W. is supported by financial support from Duke MEMS. We thank Prof Zhigang Suo for suggesting the possibility of creasing instability in polymers bonded on electrodes.

*To whom correspondence should be addressed.
xz69@duke.edu

[1] L. A. Dissado and J. C. Fothergill, *Electrical Degradation and Breakdown in Polymers* (Peter Peregrinus, Ltd., London, 1992).
[2] B. J. Chu *et al.*, Science **313**, 334 (2006).
[3] R. Pelrine *et al.*, Science **287**, 836 (2000).
[4] X. H. Zhao and Z. G. Suo, Phys. Rev. Lett. **104**, 178302 (2010).
[5] S. J. A. Koh, X. H. Zhao, and Z. G. Suo, Appl. Phys. Lett. **94**, 262902 (2009).
[6] E. Schaffer *et al.*, Nature (London) **403**, 874 (2000).
[7] M. D. Morariu *et al.*, Nature Mater. **2**, 48 (2002).
[8] S. Y. Chou, L. Zhuang, and L. J. Guo, Appl. Phys. Lett. **75**, 1004 (1999).
[9] N. Arun *et al.*, Phys. Rev. Lett. **102** (2009).
[10] N. Arun *et al.*, Adv. Mater. **18**, 660 (2006).
[11] V. Shenoy and A. Sharma, Phys. Rev. Lett. **86**, 119 (2001).
[12] X. H. Zhao, S. Q. Cai, and Z. G. Suo (to be published).
[13] K. H. Stark and C. G. Garton, Nature (London) **176**, 1225 (1955).
[14] See supplemental material at http://link.aps.org/supplemental/10.1103/PhysRevLett.106.118301.
[15] J. Blok and D. G. Legrand, J. Appl. Phys. **40**, 288 (1969).
[16] A. Ghatak and A. L. Das, Phys. Rev. Lett. **99**, 076101 (2007).
[17] E. Hohlfeld and L. Mahadevan, Phys. Rev. Lett. **106**, 105702 (2011).
[18] A. N. Gent and I. S. Cho, Rubber Chem. Technol. **72**, 253 (1999).
[19] P. M. Reis *et al.*, Phys. Rev. Lett. **103** (2009).
[20] S. Cai *et al.*, Soft Matter **6**, 5770 (2010).
[21] T. Tanaka *et al.*, Nature (London) **325**, 796 (1987).
[22] H. Tanaka *et al.*, Phys. Rev. Lett. **68**, 2794 (1992).
[23] J. Kim, J. Yoon, and R. C. Hayward, Nature Mater. **9**, 159 (2009).
[24] X. H. Zhao, W. Hong, and Z. G. Suo, Phys. Rev. B **76**, 134113 (2007).
[25] Kanellop.Ag and M. J. Owen, Trans. Faraday Soc. **67**, 3127 (1971).
[26] Date sheets of Sylguard 184 and Kapton.
[27] W. Hong, X. H. Zhao, and Z. G. Suo, Appl. Phys. Lett. **95**, 111901 (2009).
[28] W. H. Wong *et al.*, Soft Matter **6**, 5743 (2010).
[29] X. H. Zhao and Z. G. Suo, Appl. Phys. Lett. **91**, 061921 (2007).
[30] R. Huang, Appl. Phys. Lett. **87**, 151911 (2005).
[31] L. F. Pease and W. B. Russel, J. Non-Newtonian Fluid Mech. **102**, 233 (2002).
[32] A. Biot, Appl. Sci. Res., Sect. A **12**, 151 (1963).